Time-lapse traveltime shifts above compacting reservoirs: 3D solutions for prestack data

Rodrigo Felício Fuck, Center for Wave Phenomena, Colorado School of Mines; Andrey Bakulin, Shell International E & P; and Ilya Tsvankin, Center for Wave Phenomena, Colorado School of Mines*

Summary

Time-lapse (4D) traveltime shifts of reflection events recorded above hydrocarbon reservoirs can be used to monitor production-related compaction and pore-pressure changes. Existing methodology, however, is largely limited to zero-offset rays and cannot be applied to time shifts measured on prestack seismic data. Here, we obtain traveltime shifts by employing first-order perturbation theory that accounts for the stress-induced anisotropic velocity field, as well as for the deformation of reflectors. The resulting closed-form expression can be efficiently used for 3D numerical modeling of traveltime shifts and, ultimately, for reconstructing the heterogeneous stress distribution around compacting reservoirs.

The analytic results are applied to a 2D model that includes a rectangular resevoir embedded in an initially homogeneous and isotropic medium. The computed velocity changes around the reservoir are caused primarily by the deviatoric stresses and produce an anisotropic medium with substantial values of the Thomsen parameters ϵ and δ and variable orientation of the symmetry axis. The offset dependence of traveltime shifts should play a crucial role in estimating the anisotropy parameters and the compaction-related deviatoric stress components.

Introduction

Hydrocarbon production induces pore-pressure changes and compaction inside reservoirs, which causes accumulation of excess stress throughout the section. The excess stress modifies the elastic properties in and around the reservoir, and the corresponding velocity changes can be estimated using reflection traveltimes recorded in time-lapse surveys. Traveltime shifts estimated on stacked seismic data above horizontally layered media have been successfully used to delineate compartments in reservoirs (e.g., Hatchell et al., 2003; Landrø and Stammeijer, 2004). However, the existing theory breaks down in the presence of dip and cannot be applied to prestack data (i.e., to nonzero offsets).

Here, we present a 3D analytic description of stress-related traveltime shifts for rays propagating along arbitrary trajectories in heterogeneous anisotropic media. Taking heterogeneity and anisotropy into account is necessary for an adequate physical description of offset-dependent traveltime shifts. Indeed, the excess stress field created by compaction is anisotropic (in general, it is triaxial), with the magnitude of the stress components varying spatially around the reservoir.

Analytic expressions for traveltime shifts

Assuming that reservoir compaction produces only small changes in the traveltimes of seismic waves, stress-related traveltime shifts can be expressed through small perturbations of both the stiffness coefficients and the geometry of reflectors. To the first order, these perturbations can be obtained by applying Hamilton's principle of least action and considering rays propagating in an isotropic background model (Červený, 2001):

$$\delta t = \mathbf{p}\cdot\delta\mathbf{x}\Big|_{\tau_1}^{\tau_2} - \int_{\tau_1}^{\tau_2}\Delta\mathcal{H}\,\mathrm{d}\tau\,, \qquad (1)$$

where $\mathbf{p}$ is the slowness vector of the reference ray traced in the background medium, $\delta\mathbf{x}$ is the first-order variation of the position vector of the reference ray in 3D Cartesian coordinates, $\Delta\mathcal{H}$ is the corresponding variation of the system's Hamiltonian and τ is the integration parameter along the reference ray. The Hamiltonian $\mathcal{H}$ for P-waves can be expressed by the scaled eikonal equation (e.g., Červený, 2001), in which the integration parameter τ represents the traveltime along the reference ray:

$$\mathcal{H}(\mathbf{x},\mathbf{p}) = \frac{1}{2}\left[V^2(\mathbf{x},\mathbf{p})\,p_k\,p_k - 1\right] = 0\,, \qquad (2)$$

where $V(\mathbf{x},\mathbf{p})$ is the phase velocity; summation over repeated indices is implied throughout the abstract.

The first term in equation 1 can be used to account for 3D deformation of reflectors in a layered medium. Following Farra and Le Bégat (1995), we transform every point where the reference ray crosses an interface or reflects from it (i.e.,"scattering points") into a new endpoint. By applying equation 1 sequentially to all N scattering points (excluding the source and receiver positions) along the ray, we find:

$$\delta t = \delta t^e + \sum_i^N \delta t^i - \int_{\tau_1}^{\tau_2}\Delta\mathcal{H}d\tau\,, \qquad (3)$$

where

$$\delta t^e = \mathbf{p}\cdot\delta\mathbf{x}\Big|_{\tau_1}^{\tau_2}, \quad \delta t^i = (\grave{\mathbf{p}} - \acute{\mathbf{p}})\cdot\delta\mathbf{x}\,. \qquad (4)$$

Here, δt^e is the contribution of the changes in the source and receiver positions, while δt^i accounts for the variation of the interface position and is proportional to the difference between the slowness vectors of the reference ray on both sides of the interface.

As discussed above, reservoir compaction causes the velocity field around the reservoir to become both heterogeneous and anisotropic. The corresponding perturbation of the Hamiltonian for P-waves can be obtained from the Christoffel equation under the assumption that reference rays are traced in an isotropic medium (Červený, 2001):

$$\Delta\mathcal{H} = \frac{1}{2}\frac{\Delta a_{ijkl}(\mathbf{x})\, n_i n_j n_k n_l}{V^2(\mathbf{x})}\,, \tag{5}$$

where Δa_{ijkl} are the perturbations of the density-normalized stiffness coefficients, and n_i are the components of the unit slowness vector.

Relationship between the excess stress and velocity changes

Equations 3 and 5 provide the basis for describing traveltime shifts in and around compacting reservoirs. To express the elements Δa_{ijkl} in terms of the strains and excess stresses caused by reservoir compaction, we use the nonlinear theory of elasticity (e.g., Thurston and Brugger, 1964). Assuming small compaction-related static strain changes Δe_{mn}, the stiffness tensor $\mathbf{C}$ of the deformed medium can be written in the form of a Taylor series expansion:

$$\mathbf{C} = \mathbf{C}^\circ + \frac{\partial \mathbf{C}^\circ}{\partial e_{mn}}\Delta e_{mn}\,, \tag{6}$$

where $\mathbf{C}^\circ = c^\circ_{ijkl}$ is the stiffness tensor before deformation. The term $\frac{\partial \mathbf{C}^\circ}{\partial e_{mn}}$ is represented by the sixth-order tensor c_{ijklmn}, which measures the sensitivity of the stiffnesses c°_{ijkl} to the deformation Δe_{mn}. By keeping the medium density ρ constant and using linear Hooke's law to express Δe_{mn} through the compaction-related stress ΔS_{mn}, we obtain the density-normalized stiffnesses needed in equation 5 (Sarkar et al., 2003):

$$\Delta a_{ijkl} = \rho^{-1} c_{ijklmn}\left(c^\circ_{mnpq}\right)^{-1}\Delta S_{pq}\,. \tag{7}$$

Traveltime shifts due to compaction

The results by Prioul et al. (2004) indicate that the tensor c_{ijklmn} can be treated as isotropic for most applications in exploration and reservoir geophysics. Then, the stress sensitivity is described by just three independent coefficients – C_{111}, C_{112} and C_{155}. (We use capital letters to denote elements of matrices obtained from tensors by applying Voigt notation; for example, $C_{155} = c_{113131} = c_{111313}$, and $C^\circ_{44} = c^\circ_{2323}$.) Substituting equations 7 and 5 into equation 3, we obtain an explicit expression for the traveltime shifts:

$$\delta t = \underbrace{\delta t^e + \sum_{i=1}^{N}\delta t^i}_{geom.} \underbrace{- \frac{1}{2}\int_{\tau_1}^{\tau_2}\left[B_1\Delta e_{kk} + B_2\left(\mathbf{n}^{\mathsf{T}}\Delta\sigma\,\mathbf{n}\right)\right]\mathrm{d}\tau}_{vel.}\,; \tag{8}$$

$$B_1 = \frac{1}{3C^\circ_{33}}\left(C_{111} + 2C_{112}\right)\,, \quad B_2 = 2\frac{C_{155}}{C^\circ_{33}C^\circ_{44}}\,. \tag{9}$$

Here, Δe_{kk} is the trace of the excess strain tensor and $\Delta\sigma$ is the tensor of deviatoric stress given by

$$\Delta\sigma_{ij} = \Delta S_{ij} - \frac{1}{3}\Delta S_{kk}\delta_{ij}\,, \tag{10}$$

where δ_{ij} is Kronecker's symbol. Typically, the main contribution to δt is made by the velocity changes (the last term in equation 8 labeled "vel"). Indeed, for the geometric changes (label "geom") to produce a traveltime shift of at least 1 ms, an unlikely set of conditions have to take place: the displacements should be on the order of meters, the slowness contrasts cannot be smaller than 10^{-2} s/km throughout the model, and summation should include from 10 to 100 scattering points. In most typical cases, however, the displacements throughout the section are on the order of centimeters, while there is little room to increase the number of reflection/transmission points without reducing the slowness contrasts.

According to equation 8, the traveltime shifts caused by the velocity changes are given by the average of the isotropic ($B_1\Delta e_{kk}$) and anisotropic ($B_2\,\mathbf{n}^{\mathsf{T}}\Delta\sigma\,\mathbf{n}$) terms computed along the raypath. According to our sign convention, negative strains denote contraction, while positive strains denote extension (the same convention applies to stress). This means that the coefficient C_{155} and the combination $(C_{111}+2C_{112})$ should be negative, which agrees with the experimental results of Sarkar et al. (2003) and Prioul et al. (2004). Then, according to equation 8, contraction leads to an increase in velocity, which results in negative traveltime shifts. In contrast, extension causes velocity decrease and positive traveltime shifts.

To clarify how equation 8 generalizes existing results, we note that for zero-offset rays it reduces to the equation of Hatchell and Bourne (2005):

$$\delta t(x=0) = 2\int_0^Z\left[1 + \frac{1}{2}\left(R_1 + R_2\right)\right]\frac{\Delta e_{33}}{V(x_3)}\,\mathrm{d}x_3\,, \tag{11}$$

where the integration is performed over depth, and

$$\Delta e_{33}R_1 = -B_1\left(\Delta e_{11} + \Delta e_{33}\right)\,, \tag{12}$$

$$\Delta e_{33}R_2 = -B_2\Delta\sigma_{33}\,. \tag{13}$$

Therefore, our formalism provides an explicit analytic representation of the ratio $R = (R_1 + R_2)/2$ used by Hatchell and Bourne (2005) to compare the contributions of the velocity and geometric changes to the traveltime shifts. Note that the term $\Delta e_{33}/V(x_3)$ in equation 11 represents the contribution of the geometric changes, which are described by the terms δt^e and $\sum_{i=1}^N \delta t^i$ in equation 8.

Numerical tests

To illustrate the magnitude and spatial variations of traveltime shifts in prestack data, we applied equation 8 to a 2D model that includes a rectangular reservoir embedded in a homogeneous isotropic halfspace (Figure 1). Since

the overburden does not contain medium interfaces, the traveltime shifts are due primarily to the stress-induced velocity changes. The pore-pressure drop was confined to the reservoir, and the resulting excess stress and strain were computed using analytic expressions adapted from Hu (1989). The strain was confined to the incidence plane $[x, z]$, with no deformation in the y-direction ($\Delta e_{12} = \Delta e_{22} = \Delta e_{23} = 0$).

For the plane strain problem treated here, the stress tensor is triaxial, so the 3D stress-induced velocity field has orthorhombic symmetry. The velocity function in the $[x, z]$-plane, however, can be described by a heterogeneous transversely isotropic model with a tilted symmetry axis. Using the perturbations of the stiffness coefficients, we computed the stress-related Thomsen parameters and the rotation angle of the symmetry axis from the vertical (Figure 2). Because the stress-sensitivity tensor and the background medium are isotropic, the resulting anisotropy is elliptical, and $\epsilon = \delta$. The δ-values in and near the reservoir reach 0.1, which indicates that the stress-induced anisotropy is non-negligible even for the relatively small pressure drop (10 MPa) used in the test. Close to the corners of the reservoir, accumulation of the shear stress $\Delta\sigma_{13}$ causes a substantial rotation of the symmetry axis (up to 45°). Hence, in 3D the stress-induced anisotropy is described by a tilted orthorhombic model.

Figure 3 helps to compare the contributions of the deviatoric stress and volumetric changes to the traveltime shifts. Clearly, for the homogeneous background model used in the test, the shifts are caused primarily by the deviatoric stress, which makes the medium anisotropic. Since the deviatoric stress changes are symmetric with respect to the reservoir, so are the traveltime shifts for the shot in Figure 3, both in offset and depth. The influence of the shot position relative to the center of the reservoir on the total traveltime shifts is illustrated by Figure 4. As the shot moves away from the center of the reservoir, the traveltime shifts increase at longer offsets and are confined to the reservoir and deeper horizons.

The traveltime shifts in Figures 3 and 4 are also influenced by the interplay between the incidence angle θ (i.e., the slowness direction $\mathbf{n}$) and the deviatoric stress components $\Delta\sigma_{ij}$. In particular, for 2D propagation in the $[x, z]$ plane, the anisotropic velocity term in equation 8 can be written as

$$\mathbf{n}^{\mathsf{T}} \Delta\sigma \mathbf{n} = \Delta\sigma_{11} \sin^2\theta + \Delta\sigma_{13} \sin 2\theta + \Delta\sigma_{33} \cos^2\theta \,.$$

For the shot in Figure 3, the shifts are mostly generated at near offsets (i.e., for small angles θ), so the dominant excess stress component is $\Delta\sigma_{33}$. In contrast, for the shots in Figure 4, the contributions of $\Delta\sigma_{11}$ and $\Delta\sigma_{13}$ are more significant because these stress components are responsible for the traveltime shifts at moderate and large offsets.

Conclusions

The main result of our analytic developments is equation 8, which provides a framework for modeling 3D offset-dependent traveltime shifts associated with the heterogeneous, anisotropic velocity field caused by reservoir compaction. Stress-induced traveltime shifts are caused by two independent first-order phenomena: geometric and velocity changes, with the latter usually being the dominant component. The velocity-related traveltime shifts can be further separated into the isotropic term controlled by the hydrostatic stress and the anisotropic term that depends on the deviatoric stress.

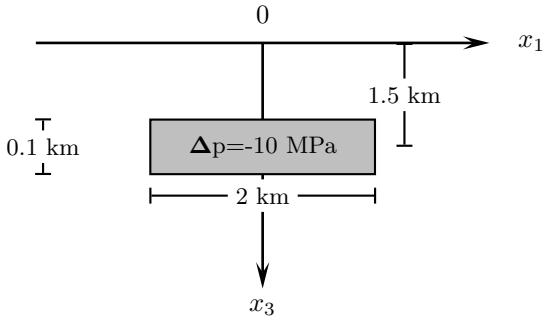

Fig. 1: 2D model of a rectangular reservoir embedded in an isotropic homogeneous medium. The pressure drop inside the reservoir is 10 MPa. The medium parameters are taken from the laboratory results of Sarkar et al. (2003) for Berea sandstone: $V_P = 2.3$ km/s, $V_P/V_S = 1.58$, $\rho = 2.14$ g/cc, $C_{111} = -13904$ GPa, $C_{112} = 533$ GPa and $C_{155} = -3609$ GPa. To compute the excess stress, we set the Biot-Willis coefficient α to 0.85 (the closer α is to unity, the more stress is generated by reducing the pore pressure in the reservoir). To simulate the static stiffnesses, V_P was scaled down by 10%, which represents a typical number for well-consolidated rocks with low porosity (Yale and Jamieson, 1994).

Although our numerical results are obtained for a simple 2D model, they illustrate several important properties of stress-induced variations in reflection traveltimes. First, traveltime shifts are associated primarily with stress-induced anisotropy and, therefore, should be estimated on prestack data. Second, the magnitude of the anisotropy parameters may be substantial, and the orientation of the symmetry axis rapidly varies in space around the reservoir corners. Third, the modeling helps to understand the complex spatial distribution of traveltime shifts caused by the interplay between the propagation direction and different stress components. On the whole, adding an extra dimension (offset) to time-lapse analysis should help to better constrain the geomechanical changes around depleting blocks and improve interpretation of 4D seismic data.

One of the main practical difficulties in modeling and interpretation of compaction-related traveltime shifts is their dependence on the sixth-order stress-sensitivity tensor. Our analytic results, obtained under the simplifying assumption that this tensor is isotropic, include two independent stress-sensitivity elements. Reliable constraints on these elements should be provided by laboratory measurements of stress sensitivity of reservoir rocks.

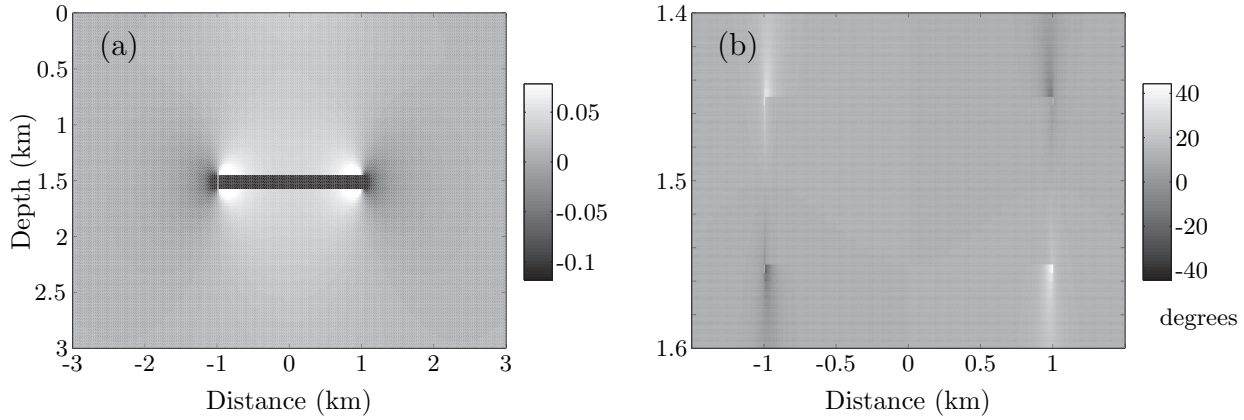

Fig. 2: Reservoir compaction makes the model in Figure 1 heterogeneous and anisotropic. (a) The anisotropy parameter $\delta = \epsilon$; (b) the angle between the symmetry axis and the vertical (positive angles correspond to counterclockwise rotation).

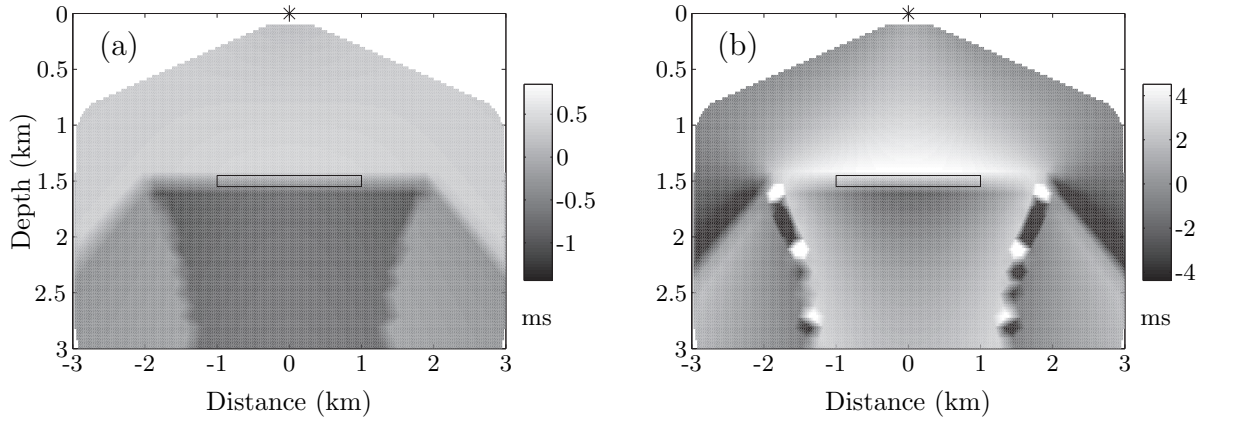

Fig. 3: Traveltime shifts for the model from Figure 1 caused by the volumetric changes (a) and deviatoric stress changes (b). The shot location is marked by the asterisk. The shifts plotted at each (x, z) point would be recorded at the receiver $(x, 0)$ for a ray reflected from an imaginary horizontal interface at depth z.

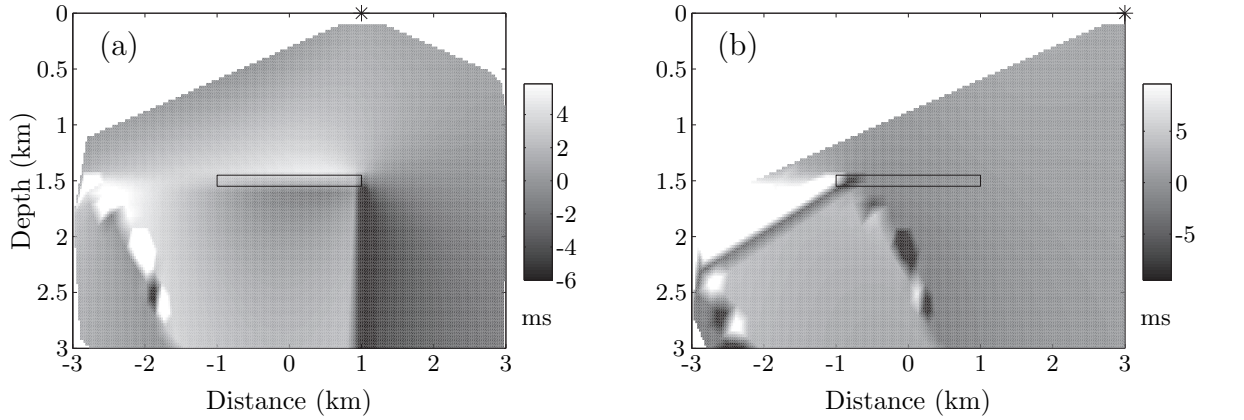

Fig. 4: Influence of the shot position (marked by the asterisk) on the total traveltime shifts for the model from Figure 1.

EDITED REFERENCES

Note: This reference list is a copy-edited version of the reference list submitted by the author. Reference lists for the 2007 SEG Technical Program Expanded Abstracts have been copy edited so that references provided with the online metadata for each paper will achieve a high degree of linking to cited sources that appear on the Web.

REFERENCES

Cerveny, V., 2001, Seismic ray theory: Cambridge University Press.

Farra, V., and S. Le Begat, 1995, Sensitivity of qP-wave traveltime and polarization vectors to heterogeneity, anisotropy and interfaces: Geophysical Journal International, 121, 371–384.

Hatchell, P., and S. Bourne, 2005, Rocks under strain: Strain-induced time-lapse time-shifts are observed for depleting reservoirs: The Leading Edge, 24, 1222–1225.

Hatchell, P., A. van den Beukel, M. Molenaar, K. Maron, C. Kenter, J. Stammmeijer, J. van der Velde, and C. Sayers, 2003, Whole earth 4D: Reservoir monitoring geomechanics: 73rd Annual International Meeting, SEG, Expanded Abstracts, 1330–1333.

Hu, S. M., 1989, Stress from a parallelepipedic thermal inclusion in a semispace: Journal of Applied Physics, 66, 2741–2743.

Landro, M., and J. Stammeijer, 2004, Quantitative estimation of compaction and velocity changes using 4D impedance and traveltime changes: Geophysics, 69, 949–957.

Prioul, R., A. Bakulin, and V. Bakulin, 2004, Nonlinear rock physics model for estimation of 3D subsurface stress in anisotropic formations: Theory and laboratory verification: Geophysics, 69, 415–425.

Sarkar, D., A. Bakulin, and R. L. Kranz, 2003, Anisotropic inversion of seismic data for stressed media: Theory and a physical modeling study on Berea sandstone: Geophysics, 68, 690–704.

Thurston, R. N., and K. Brugger, 1964, Third-order elastic constants and the velocity of small amplitude elastic waves in homogeneously stressed media: Physical Review, 133, A1604–A1610.

Yale, D. P., and W. H. Jamieson Jr., 1994, Static and dynamic mechanical properties of carbonates, in P. P. Nelson, and S. E. Laubach, eds., Rock mechanics models and measurements challenges from industry: Proceedings of the 1st North American Rock Mechanics Symposium, 463–471.